Journal of Power Sources 196 (2011) 9407–9418

Contents lists available at ScienceDirect

Journal of Power Sources

journal homepage: www.elsevier.com/locate/jpowsour

Optimization of polymer electrolyte membrane fuel cell flow channels using a genetic algorithm

Glenn Catlin, Suresh G. Advani, Ajay K. Prasad*

Center for Fuel Cell Research, Department of Mechanical Engineering, University of Delaware, Newark, DE 19716, United States

ARTICLE INFO

Article history:
Received 24 March 2011
Received in revised form 21 June 2011
Accepted 22 June 2011
Available online 29 June 2011

Keywords:
PEMFC
Single serpentine
Channel geometry
Genetic algorithm
Optimization
Finite element analysis

ABSTRACT

The design of the flow channels in PEM fuel cells directly impacts the transport of reactant gases to the electrodes and affects cell performance. This paper presents results from a study to optimize the geometry of the flow channels in a PEM fuel cell. The optimization process implements a genetic algorithm to rapidly converge on the channel geometry that provides the highest net power output from the cell. In addition, this work implements a method for the automatic generation of parameterized channel domains that are evaluated for performance using a commercial computational fluid dynamics package from ANSYS. The software package includes GAMBIT as the solid modeling and meshing software, the solver FLUENT, and a PEMFC Add-on Module capable of modeling the relevant physical and electrochemical mechanisms that describe PEM fuel cell operation. The result of the optimization process is a set of optimal channel geometry values for the single-serpentine channel configuration. The performance of the optimal geometry is contrasted with a sub-optimal one by comparing contour plots of current density, oxygen and hydrogen concentration. In addition, the role of convective bypass in bringing fresh reactant to the catalyst layer is examined in detail. The convergence to the optimal geometry is confirmed by a bracketing study which compares the performance of the best individual to those of its neighbors with adjacent parameter values.

1. Introduction

A polymer electrolyte membrane fuel cell (PEMFC) is a device that converts the chemical energy of hydrogen directly into electrical energy. The main components of a PEMFC are assembled in a layered configuration as shown in Fig. 1. The central layer is the proton exchange membrane (PEM) which is coated with catalyst layers on either side that serve as the sites for the oxidation (anode) and reduction (cathode) reactions. On either side of the catalyst-coated membrane are gas diffusion layers (GDL) comprised of porous carbon paper that are used to deliver the reactant gases (hydrogen and oxygen) to the electrodes from the supply channels in the bipolar plates which are the outermost layers of the assembly. The flow channels simultaneously remove product water from the fuel cell. The bipolar plates also collect current from the fuel cell and serve as the anode and cathode terminals. They are typically made of graphite, composites, or stainless steel for considerations of cost, structural rigidity, thermal conductivity, and electrical conductivity. Depending on the material of the bipolar plate, the flow channels are machined, molded or stamped. Ribs located between adjacent channels are responsible for making electrical contact with the GDL, which is itself in direct contact with the electrode. The contact region between the ribs and the GDL is known as the land area. The GDL is typically 0.2–0.3 mm thick and serves the purpose of evenly distributing the reactants to the catalyst layers while also creating electrical contact, and cushioning the membrane electrode assembly (MEA) against the clamping pressure under the lands.

The anode and cathode half-cell reactions are shown in Fig. 1. Although the ideal voltage for this type of fuel cell is 1.23 V, various loss mechanisms reduce the practical operating voltage to about 0.6 V. The main loss mechanisms include activation loss, ohmic loss, and mass transport loss. Activation loss is a result of slow reaction kinetics, especially at the cathode. Ohmic loss is due primarily to the resistance to proton flow in the membrane, as well as the electrical resistance of the bipolar plates and the various interconnects within the cell. Mass transport loss is typically noticed at high current draws due to fuel starvation and possible flooding. Running the fuel cell at higher stoichiometries can alleviate mass transport losses, but at the cost of higher parasitic pumping losses.

The focus of this research is on the geometric design of the bipolar plates of the cell. As stated earlier, flow channels within these plates deliver the reactants to the catalyst layers, while also removing the products. The design of the flow channels directly impacts the transport of reactant gases to the anode and cathode catalyst layers and strongly affects cell performance. A large

* Corresponding author. Tel.: +1 302 831 2960; fax: +1 302 831 3619.
E-mail address: prasad@udel.edu (A.K. Prasad).

0378-7753/$ – see front matter © 2011 Elsevier B.V. All rights reserved.
doi:10.1016/j.jpowsour.2011.06.073

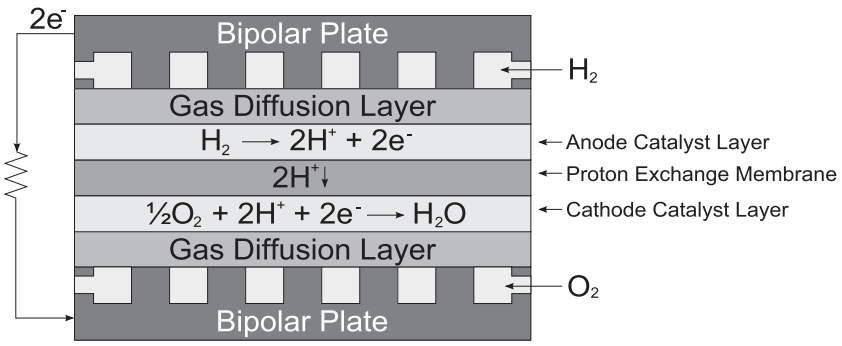

Fig. 1. Schematic cross section of a PEMFC.

focus on channel design can be found in the literature. The basic channel designs include serpentine, parallel, and interdigitated flow fields. Each basic design has its own strengths and weaknesses. Parallel channels experience the smallest pumping losses, but since the pressure drop across the length of the channels is small, they are prone to blockage by liquid water and regions of the cell become incapable of producing current. Interdigitated channels are more effective at water removal and have enhanced convective bypass into the GDL [1], but experience higher pressure drops across the cell since the inlet and outlet are not directly connected by channels. The serpentine design is quite common (see Shimpalee et al. [2]) because it is more effective at expelling liquid water thereby reducing the problem of channel flooding. In addition, the pressure difference between adjacent channels enhances convective bypass into the GDL and improves reactant delivery to the catalyst layer [1]. However, the serpentine channel experiences higher pumping losses due to its high overall channel length.

Each type of channel design is characterized by several parameters that control gas transport and impact the cell's performance. For channels of rectangular cross section, these parameters include the channel width, channel height, land width, and channel length. It is important to determine how these geometric parameters influence fuel cell performance in order to design efficient fuel cells. The selection of values for these parameters has been the subject of many research investigations and has been explored experimentally, numerically, and analytically. For example, a study on land-to-channel width ratio was done by Yan et al. [4]. Tapering the width continuously between the inlet and outlet was investigated by Yan et al. [5]. Xu and Zhao [6] developed a convection-enhanced serpentine flow field (CESFF) by forcing a single channel to double back on itself. All of these examples identify the optimal parameters for a cell of given dimensions and tend to generalize that these parameters can be used to design fuel cells of larger dimensions.

Performance improvements obtained by designing cells that make highly effective use of a given nominal area can lower the cost of fuel cells which will promote their commercialization. The goal of the current work is to devise a method that can rapidly optimize the geometric design of a flow field that maximizes the net power output for an active area of given dimensions. Our optimization method employs a genetic algorithm to efficiently determine the optimal channel geometry within a relatively large search space. The effectiveness of a specific fuel cell is evaluated by a fitness function whose value is the net power per unit area, or net power density. A set of in-house scripts was developed to combine the strengths of finite element analysis (FEA) with a parameterized solid model drawing script and a genetic algorithm optimization method. The channel designs are considered for a specific nominal area and for a specific set of operating conditions. The principal contribution of this work is the automated optimization method to efficiently determine the best channel design for a PEMFC of a given size.

2. PEMFC model

In order to minimize the costs associated with the design and optimization of an individual cell, it is valuable to attain predictive capability regarding the cell's performance potential before actual construction and testing. It is therefore beneficial to include numerical modeling in the PEMFC design process. Many works have been dedicated to the construction of numerical models that can accurately predict PEMFC performance. These models have increased in complexity over time, evolving from two-dimensional models by Chen et al. [7], to relatively complex three-dimensional models. Such complex models have been created by different groups including Le and Zhou [8] who included multiphase flow, Shimpalee et al. [2], and Fan et al. [9]. These researchers have constructed their own in-house CFD models or used commercially available codes. For our analysis we use a commercially available software package (FLUENT 6.3.26).

2.1. Model assumptions

The ANSYS software package FLUENT and the FLUENT PEM fuel cell module is used in this research to compile the appropriate user-defined functions for a PEMFC. This model does not take into account areas of importance such as material degradation, the presence of impurities in the reactant supply streams, and non-ideal operating conditions such as variances in control system responses and the non-isothermal nature of the environment which the fuel cell is bound to experience during operation. Each of those factors would lead to reduced fuel cell performance. Despite these limitations on the absolute accuracy of the predicted performance, it is sufficient to obtain the relative performance of the various cell configurations for the purposes of this study. Likewise, product water is assumed to remain exclusively in vapor state in this model. This limitation is also acceptable for our purpose as the chosen operating condition is sufficiently removed from the flooding regime. The PEMFC model used in this research assumes that the flow is laminar, the fluid is incompressible, the inlet gases follow the ideal gas law, the gas diffusion layers, catalyst layers, and membrane layer are isotropic materials, the flow is single phase, and that steady-state conditions exist. The experimental results obtained by Spernjak et al. [10] in the Fuel Cell Research Laboratory at the University of Delaware will be used to verify the PEMFC model's results in a later section.

2.2. Governing equations

Reactant transport is strongly influenced by the geometry of the reactant flow channels in a PEMFC. The important governing equations are described below, beginning with the conservation of mass equation:

$$\frac{\partial \rho}{\partial t} + \nabla \cdot (\rho \mathbf{v}) = S_m \tag{1}$$

Eq. (1) is valid for mass balance in the channels as well as the GDL where both diffusion and convection are important. S_m is the mass source term and for all zones in this model $S_m = 0$.

Next, the momentum equation is used to solve for the fluid velocities in the channels and the GDL and the species' partial pressures:

$$\frac{\partial \rho \mathbf{v}}{\partial t} + \nabla \cdot (\rho \mathbf{v}\mathbf{v}) = -\nabla p + \nabla \cdot \tau + S_M \tag{2}$$

The momentum source term, S_M, is zero in all zones except for the gas diffusion layers and the catalyst layers. In these zones, the Darcy equation is used to define S_M.

$$S_M = -\frac{\mu}{K}\varepsilon \mathbf{v} \tag{3}$$

Here, μ is the viscosity of the fluid, and K and ε are the permeability and porosity, respectively, of the particular zone.

Temperature is modeled through the energy equation whose general form is as follows:

$$\frac{d}{dt}[\varepsilon \rho h + (1-\varepsilon)\rho_s h_s] + \nabla \cdot (\rho \mathbf{v} h) = \nabla \cdot \left(k_{eff} \nabla T - \sum_j h_j J_j \right) + S_h \tag{4}$$

where h is the enthalpy of the gas mixture, J is the diffusive flux, the subscript j represents the chemical species of the bracketed quantity, and the subscript s represents the solid phase of the bracketed quantity. Zones with solid phases include the GDL, CL, membrane, and the bipolar plate. The first two terms on the right hand side of Eq. (4) are the conduction and species diffusion terms, respectively. S_h is the volumetric source term and is defined for all zones of the cell by:

$$S_h = I^2 R_{ohm} + h_{reaction} + \eta R_{an,cat} + h_{phase} \tag{5}$$

where $I^2 R_{ohm}$ is the ohmic heating term, $h_{reaction}$ is the heat of formation of water term, ηR is the electric work term (η and R are the activation loss and volumetric transfer current, respectively), and h_{phase} is the latent heat of water term. The effective thermal conductivity is calculated as:

$$k_{eff} = \varepsilon k_f + (1-\varepsilon) k_s \tag{6}$$

where the subscripts f and s represent the fluid and solid component, respectively, of a specific zone.

The heterogeneous reactions that take place on the catalyst surfaces are balanced by their rate of production as described below:

$$\frac{\rho D_j}{\delta}(y_{j,surf} - y_{j,cent})r = \frac{M_{w,j}}{nF} R_{an,cat} \tag{7}$$

where D_j is the effective mass diffusivity, r is the surface to volume ratio of the catalyst layer, δ is the average distance between reaction surfaces and cell center, y is the mass fraction of species, and the subscripts j,*surf* and j,*cent* refer to the surface and the center of the cell, respectively. $M_{w,j}$ is the molecular weight of the species, n represents the number of electrons transferred per molecule and F is the Faraday number.

The conservation of species is required to calculate the mass balance for each of the involved reactants in this model and is defined below:

$$\frac{\partial(\varepsilon \rho y_j)}{\partial t} + \nabla \cdot (\rho \mathbf{v} y_j) = \nabla \cdot (\rho D_j \nabla y_j) + S_j \tag{8}$$

where S_j refers to the species source term.

The effective mass diffusivity is calculated using the expression by [11,12].

$$D_j = \varepsilon^{1.5}(1-s)^{r_s} D_j^o \left(\frac{p_o}{p}\right)^{\gamma_p} \left(\frac{T}{T_o}\right)^{\gamma_t} \tag{9}$$

The species source terms, S_j, are zero except for the fluid zones and are described by the next three equations:

$$S_{H_2} = -\frac{M_{w,H_2}}{2F} R_{an} \tag{10}$$

$$S_{O_2} = -\frac{M_{w,O_2}}{2F} R_{cat} \tag{11}$$

$$S_{H_2O} = -\frac{M_{w,H_2O}}{2F} R_{an} \tag{12}$$

The electrochemistry modeling begins by calculating the rates of hydrogen oxidation and oxygen reduction in the anode and cathode catalyst layers, respectively. The following are the two potential equations solved in the PEM model. Eq. (13) is solved for the electron transport through the solid conducting regions including the bipolar plates, gas diffusion layers and catalyst layers. Eq. (14) is solved for the proton conductivity through the membrane.

$$\nabla \cdot (\sigma_s \nabla \phi_s) + R_s = 0 \tag{13}$$

$$\nabla \cdot (\sigma_m \nabla \phi_m) + R_m = 0 \tag{14}$$

In the preceding equations, σ_s is the electrical conductivity of the respective solid zone, σ_m is the membrane electrical conductivity calculated by Eq. (15) [12], ϕ is the electric potential, and R is the volumetric transfer current.

$$\sigma_m = \beta\varepsilon(0.514\lambda - 0.26)^{\omega} e^{1268(1/303 - 1/T)} \tag{15}$$

Here, λ and ω are water content and the membrane conductivity constant, respectively. For the anode side, the source terms are defined as $R_s = -R_{an}$ and $R_m = +R_{an}$. On the cathode side, the source terms are defined as $R_s = +R_{cat}$ and $R_m = -R_{cat}$. The source terms for the unnamed zones are assumed to be equal to zero.

The terms R_{an} and R_{cat} are defined according to the Butler–Volmer equations as shown below.

$$R_{an} = j_{an}^{ref} \left(\frac{X_{H_2}}{X_{H_2}^{ref}}\right)^{\gamma_{an}} (e^{\alpha_{an} F \eta_{an}/RT} - e^{-\alpha_{cat} F \eta_{an}/RT}) \tag{16}$$

$$R_{cat} = j_{cat}^{ref} \left(\frac{X_{O_2}}{X_{O_2}^{ref}}\right)^{\gamma_{cat}} (-e^{\alpha_{an} F \eta_{cat}/RT} + e^{-\alpha_{cat} F \eta_{cat}/RT}) \tag{17}$$

The local activation losses are solved as follows:

$$\eta_{an} = \phi_s - \phi_m \tag{18}$$

$$\eta_{cat} = \phi_s - \phi_m - V_{OC} \tag{19}$$

The activation loss, η, is calculated as the difference between the solid and membrane potentials as shown above.

2.3. PEMFC material properties and boundary conditions

This section summarizes the boundary conditions and material properties that are maintained constant in the current simulations. The inlet gases are set at a constant mass flow rate of humidified hydrogen (anode side) and air (cathode side). The mass flow rates

Table 1
Material properties.

Property	Value	Property	Value
$c_{p;col,gdl,cl}$	871 J kg^{-1} K^{-1}	$\alpha_{an,cat}$	2
$c_{p;mem}$	2000 J kg^{-1} K^{-1}	β	1
D_j^o	3×10^{-5} m^2 s^{-1}	$\gamma_{an,cat}$	1
h_{gdl}	0.25 mm	γ_p	1
h_{cl}	12.5 μm	γ_t	1.5
h_{mem}	25 μm	$\varepsilon_{cl,mem}$	0.5
j_{an}^{ref}	5×10^9 Am^{-3}	$\rho_{col,cl,gdl}$	2719 kg m^{-3}
j_{cat}^{ref}	4×10^9 Am^{-3}	ρ_{mem}	1980 kg m^{-3}
$k_{p;col,gdl,cl}$	8 W m^{-1} K^{-1}	$\sigma_{cl,gdl}$	5000×10^7 ohm^{-1} m^{-1}
$k_{gdl,cl}$	1×10^{-12} m^2	σ_{col}	1.0×10^6 ohm^{-1} m^{-1}
M_m	1100 kg kmol^{-1}	σ_{mem}	1.0×10^{-16} ohm^{-1} m^{-1}
p_o	101.325 kPa	ω	1
r	4×10^9 m^{-1}		
T_o	300 K		
$X_{j,ref}$	1		

Table 2
Boundary conditions.

Location	Boundary condition type	Value
Cathode and anode inlets	Mass flow rate	[Calculated]
Anode and cathode outlets	Pressure	101325 Pa
All exterior surfaces	Temperature	353 K
Cathode terminal surface	Voltage	0.6 V
Anode terminal surface	Voltage	0.0 V

are calculated for a stoichiometry of $\lambda = 2$ at 1 A cm^{-1}. Using this condition, appropriate values for the mass fluxes are calculated based on the area of a given cell. The outlet of each channel is open to the atmosphere and set to 1 atm. The cathode terminal wall is set at a constant 0.6 V and the anode terminal wall is grounded at 0 V, and both terminal wall surfaces are set to 80 °C. Tables 1 and 2 summarize the material properties and boundary conditions employed in this PEMFC model.

2.4. Meshing strategy and convergence considerations

Building a three-dimensional solid model with an appropriately constructed mesh is an important concern when performing any type of numerical modeling and simulation routine. The mesh used here corresponds to the best practice recommendations of the FLUENT PEMFC Add-on Module. Each zone of the cell requires a specific set of meshing rules. The GDL thickness is divided into 10 mesh layers, the catalyst layer and membrane thicknesses are divided into four mesh layers, and the channel height is divided into 10 layers. The bends of each serpentine pass have the highest velocity and pressure gradients, so it is important to keep the mesh density high in these zones, but the mesh density is allowed to coarsen by a symmetric 1.1 meshing ratio along each pass. The result is that the channel ends are defined by cube shaped mesh elements, while the channel lengths are defined by slightly elongated hexagonal elements. An important feature of the meshing process used by the Gmesh script ensures that there are no skewed elements. All meshed elements are hexagonal with 90° angles between each face. An example mesh is shown in Fig. 2.

A mesh refinement study was conducted in order to show that the solution was grid independent. In particular, the mesh density was increased at the channel ends where the velocity gradients are highest. The final mesh density selected for the simulations showed negligible changes in the solution with further refinement.

The solver is based on the finite-volume method and employs a pressure-based solver with double-precision. The convergence of the model depends on several constraints. First, all the residual quantities including continuity, three velocity components, energy, hydrogen species, oxygen species, water species, electrical potential, protonic potential, and water content must attain a tolerance at or below 1×10^{-4}. The convergence criteria also require the average y-current density on the cathode and the pressure at the cathode inlet to converge to below 1×10^{-6}. The y-current density is the current density normal to the surface of the bipolar plate. These two quantities are required to determine the gross power density of the cell, and the parasitic power consumption. These values are needed in the optimization strategy and will be discussed in Section 6.

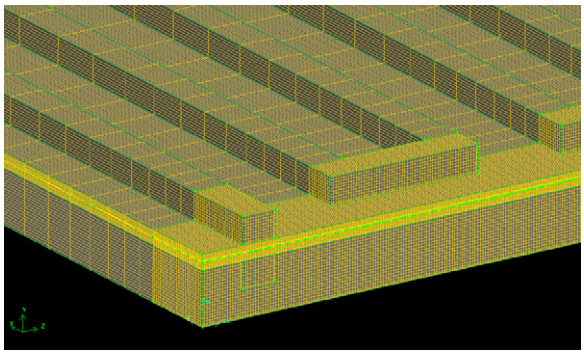

Fig. 2. Example of mesh density in the single-serpentine fuel cell domain (top bipolar plate removed in order to reveal the channel domain).

Our optimization approach requires multiple simulations with varying geometrical characteristics for the flow channels. Varying the channel geometry requires the construction of a unique model and mesh for each simulation. Therefore, an efficient and methodical way of constructing and meshing a wide variety of PEMFCs is required for this study. Drawing and meshing each unique cell would require a prohibitively large amount of time and therefore, the process was automated using a GAMBIT journal file, which will be referred to hereon as the Gscript file. GAMBIT [13] is a commercially available software package that was used in this study to create the domain of a PEMFC, divide the model into a discretized mesh, and identify the necessary boundary conditions and zones without manual input. GAMBIT outputs a mesh file that can be read by FLUENT [14] to perform a simulation at the desired operating conditions.

For the case of a single-serpentine flow field design, four parameters are needed to fully describe the design for a fixed area: channel width (CW), channel height (CH), land width (LW), and channel length (CL). The Gscript file receives these quantities as input parameters and appropriately constructs the solid model. However, in this study, CH is set to a constant value of 1.0 mm.

3. PEMFC model validation and verification

3.1. Comparison with experimental data

In order to validate the model, a comparison to an experimental result is provided in this section. The model was constructed to replicate the cell employed by Spernjak et al. [10] who used 10 cm^2 PEMFC bipolar plates made of graphite with a single-serpentine channel configuration. The channels were 0.8 mm wide, 1 mm high, and the land width was 0.8 mm. Humidified air and hydrogen were supplied at 0.18 and 0.076 slpm, respectively. The cell was set to operate at a constant temperature of 80 °C. The OCV for this verification run was set to 0.778 V to match the corresponding experimental value. The simulation was initiated by setting the voltage to OCV followed by stepwise 0.5 V decrements corresponding to the experimental data. Fig. 3 shows a good agreement between the experimental and numerical results. The small differences between the model and the experimental data are due to the assumptions made in the model. However, the overall degree of

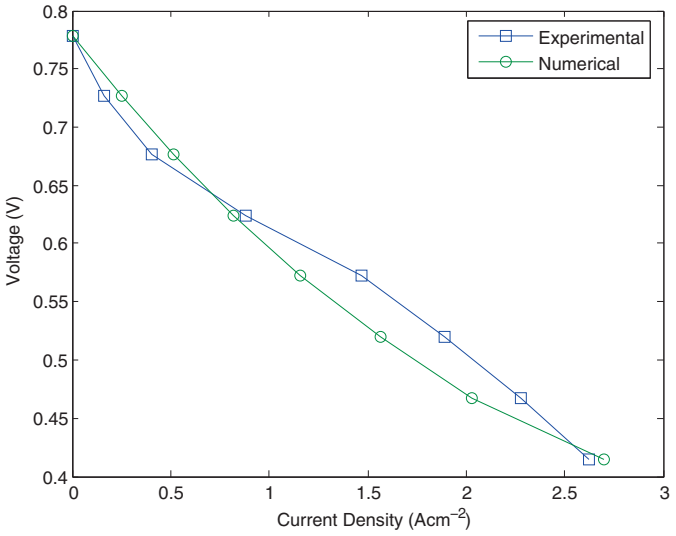

Fig. 3. Validation of PEMFC simulation model by comparing with experimental data.

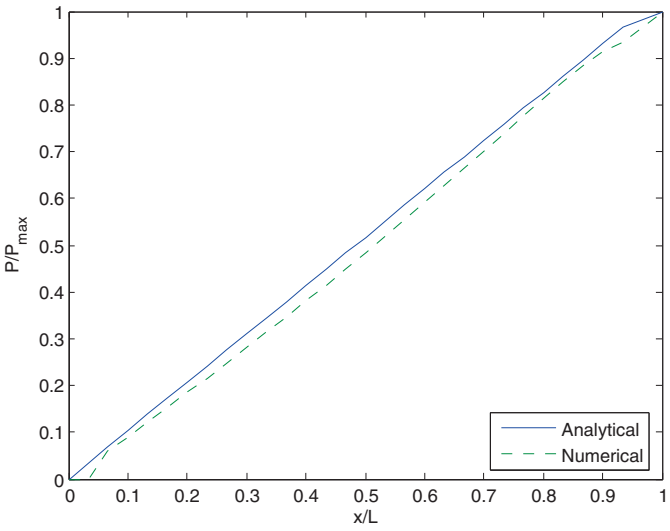

Fig. 4. Comparison of numerical and analytical PEMFC pressure distribution along the center pass.

agreement demonstrates that the model is a good approximation over the prevailing range of operating conditions.

In addition, global mass conservation was also checked to verify the model. This check was accomplished by examining simulation data for one point on the polarization curve corresponding to the operating voltage of 0.624 V. FLUENT calculates the amount of oxygen consumed by the cell and the average current flux magnitude in the y-direction at the cathode terminal wall. The total release of electrons can be directly related to the oxygen consumption rate as given below.

$$I = \frac{\dot{m}_{O_2} 4F}{M} = \frac{(6.629 \times 10^{-4})(4)(9.6485 \times 10^4)}{31.9988} = 7.995\,\text{A} \qquad (20)$$

Here, $\dot{m}$ is the oxygen consumption rate (g s^{-1}), M is the molecular mass of oxygen, and F is the Faraday constant. Next, the current density over the cathode terminal surface was integrated to obtain a total current of 7.993 A, which agrees very well with the value in Eq. (20) and confirms that mass is globally conserved.

3.2. Comparison with analytical results

Although the experimental verification shows that the model is capable of predicting overall performance values in the form of current density output versus voltage, it is necessary to further verify detailed results internal to the cell. Feser et al. [3] formulated an analytical expression that predicts the pressure distribution along the channels of the cell:

$$P(x) = \frac{\Delta P_{cell}}{2N_c}\left(\frac{\sinh(m((x/\text{CL}) - (1/2)))}{\sinh(m/2)} + 1\right) \qquad (21)$$

In this equation, ΔP_{cell} is the total pressure drop across the entire cell, N_c is the number of passes in the cell, CL is the length of a single pass, and m is a dimensionless quantity defined as $m^2 = 4(L^2 A_c^{-1})(h_{\text{GDL}}/\text{LW})(k_{ip}/k_{chan})$. In this expression, A_c is the product of the channel width and channel height, k_{ip} is the in-plane permeability of the GDL, and k_{chan} is the permeability of the channel. The channel permeability is approximated as a function of the height-to-width ratio of the channel according to Feser et al. [3].

Fig. 4 provides a comparison between the pressure distribution along the center pass predicted by the model with the analytical values provided by Eq. (21). The data in Fig. 4 have been normalized by the length (CL) of a single pass and by the maximum pressure along the pass (P_{max}). The agreement between these results provides further evidence that the model is capable of accurate predictions.

4. Optimization strategy

The genetic algorithm (GA) is an optimization technique that employs the fundamental principles that drive natural evolution and was originally developed by Holland according to Sivanandam and Deepa [15]. The strength of the GA is its ability to efficiently locate optima within relatively large search spaces. In order for a GA to be implemented, a system must first be reduced to the basic parameters that are needed to describe it. Once these parameters are identified, the GA can go to work on determining the optimum values for these parameters. The GA used in this study is the commercially available Genetic Algorithm and Direct Search Toolbox available from MatLab.

4.1. Genetic algorithm theory

The description of the GA in this research employs terms typically used when discussing genetics. An individual is defined by the genes that make up its chromosome. In this work, the chromosome is responsible for describing a unique PEMFC individual (IND). Each individual has a specific number of genes. For a three-parameter optimization, there are three genes, one for each parameter. The parameters in this research include the channel width, land width, and channel length; each parameter can assume values within an allowable range that is set by selecting an upper and lower bound.

The GA proceeds by spawning new generations, such that individuals in the current generation are created by examining and selecting genes from the individuals in the previous generation. The performance of an individual is determined by applying an appropriately formulated fitness function in the GA. The fitness function is responsible for minimizing or maximizing a quantity of interest. In the case of the PEMFC, the fitness function is defined as the net power density. The GA includes the crossover process between successive generations such that the genes of the best individuals are crossed with those of other individuals which showed good performance. The new individuals are comprised of different combinations of the genes in the previous generation. The GA also includes mutations between successive generations to help the optimization process by including values that were not present

Table 3
Genetic algorithm settings.

GA setting	Chosen setting
Crossover fraction	0.8
Stall time limit	Infinite
TolFun	1×10^{-6}
TolCon	1×10^{-6}
Creation function	Uniform
Fitness scaling function	Rank
Selection function	Stochastic uniform

during earlier generations. Random mutations help to dislodge a solution that may have settled on a local optimum and propel it towards the desired global optimum. The mutation rate is set so as to not create completely random individuals, but rather to include a limited amount of randomness between successive generations. While the method does not guarantee that the global optimum will always be found, it is generally accepted that the final solution will be close to the global optimum as long as successive generations are incapable of producing better individuals. Not finding the exact global optimum is a trade off for saving computational time and power.

The GA finds the optimum solution with far fewer simulations than an exhaustive brute force parametric study which evaluates the performance of each of a vast array of possible individuals. The MatLab GA and Direct Search Toolbox are capable of executing such a scheme along with many other options that are necessary to control a GA optimization. This toolbox is fully integrated with the automated process that optimizes a PEMFC in this research. The following sections will outline the options that guide the GA and the integration of each of the software tools that are required to automate the optimization and solution processes.

4.2. MATLAB GA Toolbox set parameters

Table 3 summarizes the GA parameters that are used throughout this study. The elite count is the number of individuals that are preserved from one generation to the next. These elite individuals are the best performers of a given generation and are used to crossover and create the rest of the population in a given generation. The crossover rate can range from zero to one and represents the fraction of the next generation that is comprised of crossover offspring. The remaining offspring are comprised of mutated individuals. The stall time limit is set to infinity in order to eliminate the possibility of terminating the PEMFC model before completing a simulation. The tolerance values are set to terminate the GA process if successive generations do not create new individuals whose performance improvement exceeds the set tolerance value. This setting would suggest that the optimum was reached and the individuals converged to the best solution within the search space. The fitness scaling function puts the individuals of a given population in rank order instead of ranking them by their fitness values. The best individual is ranked number 1, and so on. The ranking of individuals removes the effects of the spread between raw fitness scores.

4.3. Communication script

Now that the GA settings have been fully defined and the optimization process has been described, the process of evaluating an individual's fitness needs to be discussed. This study represents the first instance in which GA optimization has been coupled with an automated scheme capable of constructing unique PEMFC models and evaluating their performance. Although previous studies have investigated PEMFC performance parametrically, none have been aimed at finding the optimal channel characteristics of a customizable area. The following script is capable of automatically generating a solid model for a fuel cell of a chosen design and size. The channel geometry that produces optimum performance for a cell of a certain size need not be the same as that for a larger cell. The benefit of our script is the scalability of the process; an optimum geometry can be found for a cell of any size, automatically and efficiently. This research identifies the optimum values for a three-parameter single serpentine configuration.

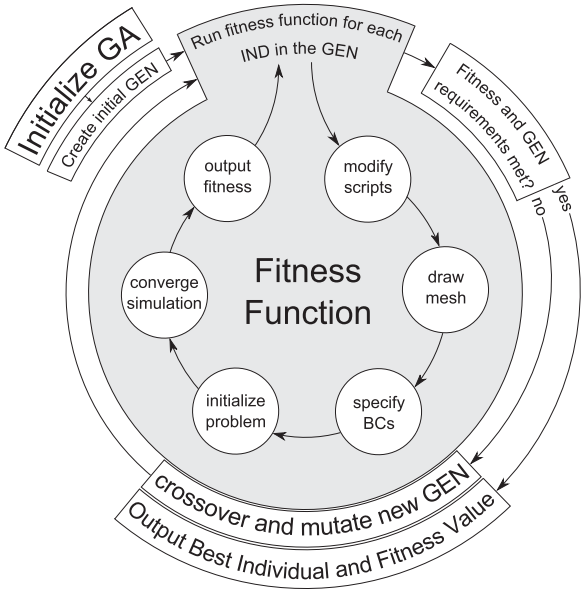

Fig. 5. Genetic algorithm flow chart.

Several scripts were written to control and integrate all of the software packages necessary to run the optimization. Fig. 5 summarizes the flow and connectivity of the various scripts. The user sets the number of parameters to be optimized as well as the upper and lower bounds for each parameter. Once the previously discussed GA options are set and the search space is chosen, the GA optimization is ready to begin.

At this point, the GA Toolbox creates random sets of parameter values for each of the individuals in the initial population. This initial population is referred to as generation (GEN) zero. The GA evaluates the fitness of each individual by calling the fitness function (FF). The fitness function is the script that was created to control the optimization and is therefore responsible for the integration of all of the software packages and extracts the appropriate data to calculate the fitness of an individual. The script calculates the fitness of each individual of the generation, one at a time. The fitness function receives as input the values for each of the genes that describe an individual. Each of the values is written to a GAMBIT journal file. The GAMBIT journal file, Gmesh, is the third script in this process. It is designed to draw a solid model according to the input parameter values. It then populates the model with an appropriately scaled mesh and applies the boundary condition types and zone types to the PEMFC domain. Once the model is fully constructed, the mesh is written to file.

The FF script next calls the FLUENT journal script, Fjou. The Fjou script is responsible for loading the PEMFC module, applying all material types to each of the zones, applying values to each of the required boundary conditions, initializing the solver, setting convergence criteria, converging the solution, and saving the desired solution values to a file. The Gmesh script takes the raw data from the Fjou output files and uses it to calculate the fitness of each individual. This final value is returned to FF and sent back to the GA

control process. This process is repeated for each of the individuals that the GA requests for each generation.

Specific strengths of the scripts are: the Gmesh script calculates the number of serpentine passes that are required to fill a given area; the Fjou script can handle any Gmesh script with appropriately named zones; and the operating conditions are easy to access if alterations are desired.

The GA terminates when the specified number of generations is reached, or when the convergence criteria for successive generations are met. The GA then outputs the best individual of the entire population along with its associated parameter values. This individual represents an optimum configuration within the search space. The individual can then be compared to other individuals in the population to extract the characteristics that strongly influenced their performance. The information gathered from the population as a whole can be used to design and initialize future GA studies in order to decrease convergence time and increase performance.

5. Results and discussion

This study uses a population of eight individuals for each generation, and a limit of 12 new generations beyond the initially generated randomized population as summarized in Table 3. Each new generation selects two elite individuals from the previous generation. These two elite individuals are used to create four additional crossover offspring. The remaining two individuals of each generation are created by the mutation function. The entire population consists of 104 individuals; however, since the elite individuals pass unchanged between generations, the number of unique individuals that need to be evaluated is equal to 80. The fitness function script prevents the reevaluation of individuals by checking a continually updated database for repeat individuals during the optimization.

The search space for the design of this PEMFC is defined by prescribing ranges of values for the three independent parameters: channel length (CL), channel width (CW), and land width (LW). The channel length is defined as the length of a single pass of the serpentine channel, as opposed to the overall length of the entire serpentine channel from inlet to outlet. The three parameters are depicted schematically in Fig. 6.

The active area of the fuel cell extends beyond the outer edges of the channel in the *xz*-plane by an amount equal to one-half of the specified land width as shown in Fig. 6. The nominal area (A) of the cell is set at a target value of 16 cm^2. The range of values for each of the parameters is as follows: $4\,cm \leq CL \leq 14\,cm$; $0.5\,mm \leq CW \leq 1.5\,mm$; and $1.0\,mm \leq LW \leq 3.5\,mm$. The channel height is set to a constant value of 1.0 mm. The Gmesh script uses the three parameter values to calculate the number of passes that are required to fill the nominal area with the given channel width, land width, and channel length. The number of passes is rounded to the nearest odd integer in order to create a cell with the desired channel configuration in which the inlet and outlet ports are on opposite sides of the cell. This condition maintains the same inlet and outlet configuration for all individuals. The PEMFC is designed with counter-current flow channels such that the inlet and outlet ports of the anode are reversed for the cathode. The anode and cathode channels overlay exactly on top of each other when projected on to the *xz*-plane.

The gross power density of a cell is the product of its current density, i, and its voltage, V. In practice, a fuel cell system incorporates the balance-of-plant consisting of several components whose input power is drawn from the fuel cell itself. The cumulative balance-of-plant power requirement represents the cell's parasitic power loss. Of particular relevance to this study, the power requirement of the motor and compressor assembly for the air supply system is largely

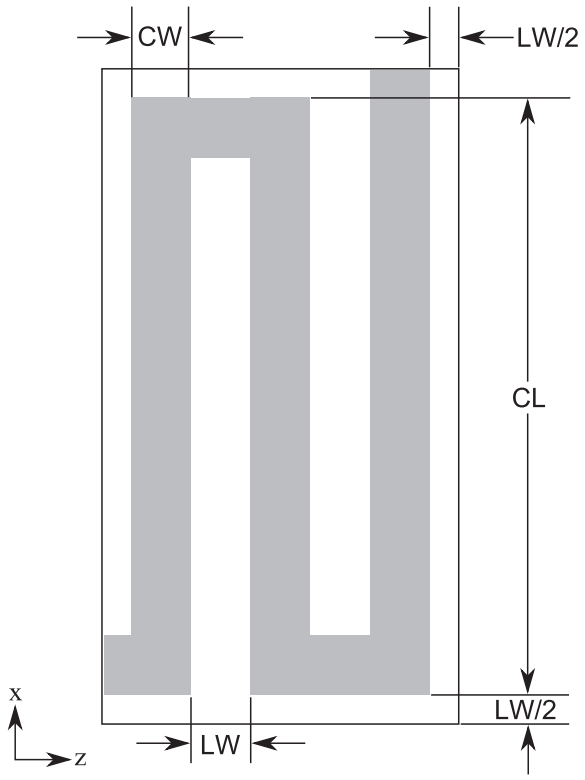

Fig. 6. Schematic of the three-parameter single-serpentine configuration.

influenced by the channel geometry. Therefore, it is appropriate to include the parasitic loss associated with driving air through the cathode channels as a factor in the fitness function. Each channel configuration within the search space imposes a power requirement that is proportional to the total pressure drop from inlet to outlet and the mass flow rate through the channel. A small channel cross-sectional area and long overall channel length results in a much higher pressure drop than a channel with a large cross-sectional area and short overall channel length. Larminie and Dicks [16] provide an expression for the parasitic power requirement of a cell:

$$P_{par} = c_p \frac{T_{amb}}{\eta} \left(\left(\frac{p_{in}}{p_{amb}} \right)^{(\gamma-1)/\gamma} - 1 \right) \dot{m} \tag{22}$$

In this equation, the combined motor and compressor efficiency $\eta = 0.7$, and the heat capacity ratio of air $\gamma = 1.4$. T_{amb} is the ambient temperature, p_{amb} is the ambient pressure, p_{in} is the pressure at the inlet of the PEMFC, and $\dot{m}$ is the mass flux of air. The inlet pressure is calculated by FLUENT and is part of the data output of the Fjou script. The mass flow rate of air is calculated using an expression from Larminie and Dicks [16]:

$$\dot{m}_{air} = 3.57 \times 10^{-7} \cdot \lambda i A \tag{23}$$

Here, i is the current density, and A is the nominal area of the cell. Similarly, the hydrogen flow rate is calculated as:

$$\dot{m}_{H_2} = 1.05 \times 10^{-8} \cdot \lambda i A \tag{24}$$

Both reactant gas mass flow rates are set to provide a stoichiometry of $\lambda = 2$ at $i = 1\,A\,cm^{-2}$, which is a common condition used when evaluating PEMFC performance. With all of the required quantities defined, the net power is now calculated in Eq. (25). The parasitic power term does not include any loss due to the supply of hydrogen to the anode side because the hydrogen is sup-

Table 4
Best and worst individual comparison.

Quantity or parameter	Best	Worst
Channel length	4.64 cm	4.0 cm
Channel width	0.762 mm	1.11 mm
Land width	0.934 mm	3.50 mm
Net power density	0.954 W cm^{-2}	0.474 W cm^{-2}

plied from a pressurized vessel, and therefore requires no external compression.

$$P_{net} = P_{cell} - P_{par} \tag{25}$$

The power of the cell, P_{cell}, is calculated by the PEMFC module and is the product of the cell's current density integrated over the nominal area and the cell voltage. The desired fitness function is finally defined as the net power per unit area.

$$\text{FF} = -\frac{P_{net}}{A} \tag{26}$$

The negative sign is included in the fitness function because the MatLab GA technique searches for the minimum in the fitness function, whereas our goal is to maximize the net power density. Once the simulation is complete, the absolute value of the fitness function represents the net power density of each individual.

5.1. Comparison of best and worst individuals

This GA optimization strategy resulted in a total of 104 individuals, 80 of which were unique. These individuals covered a wide range of parameter values within the limits set in the GA. The performance corresponds to the fitness function defined in Eq. (26). Because the fitness function is the net power density as opposed to the gross power density, the individuals are ranked more accurately on how they would perform during actual operation.

The focus of this section is on the comparison between the best and worst individuals in the population whose parameter and output values are summarized in Table 4. This comparison aids in the explanation of the physical reasons for why two individuals within a reasonable search space produce very different performance values. The net power density of the worst individual is 50.7% lower than that of the best individual.

The investigation of these individuals begins by examining the current density distributions on the surface of the cathode catalyst layer of each individual. Fig. 7 shows the current density magnitude on the cathode GDL/CL interface where the oxygen reduction reaction takes place. Areas of relatively high current density indicate a more vigorous reaction and good oxygen transport. The figure shows that the worst individual is unable to utilize the catalyst sites under the land regions of the cell, whereas the best individual makes much better use of the areas under the land. In the worst individual, the majority of the current is produced directly under the channel and is collected by the ribs of the bipolar plate. The reason for the poor utilization of active area under the lands in the worst individual is the high land width of 3.5 mm. Reactant gas is unable to diffuse laterally far under the land and results in mass transport loss leading to poor current density. It is also evident that the inlet and outlet regions do not produce much current density in either of the individuals. This is due to the counter-current flow configuration used in the cell. As a result, by the time the reactant flow reaches the outlet, reactant depletion lowers its partial pressure, which starves the region of either oxygen or hydrogen and therefore limits the reaction.

Next, we investigate the oxygen consumption within the cell. When a PEMFC cathode is fed with air instead of pure oxygen, the reaction is more likely to be limited by the oxygen content of the air between the inlet and the outlet of the cell. To understand a given cell's performance, it is important to examine the local consumption of oxygen and correlate it to the overall performance of the cell. Fig. 8 compares the best and worst individuals in terms of the oxygen concentration in the cathode channel midplane.

Fig. 8 shows that for the best individual the oxygen is almost completely depleted by the time the flow reaches the outlet. This observation confirms that oxygen consumption is high for the best individual resulting is high overall current density. On the other hand, the worst individual's outlet oxygen concentration is still quite high, about half of the inlet concentration. The main reason for this is the reduced oxygen consumption due to the channel's inability to deliver reactants to the catalyst layer underneath the wide land regions via convective bypass.

Convective bypass is the primary mechanism that delivers reactant gases to the catalyst layer under the lands. Convective bypass is proportional to the pressure difference between two adjacent channels in a cell. The largest pressure difference occurs between the ends of two adjacent channels across the root of the rib (across points A and B in Fig. 6). If sufficiently large, this pressure difference can convectively drive reactant gas into the GDL and the CL under the lands, while also driving out product water from under

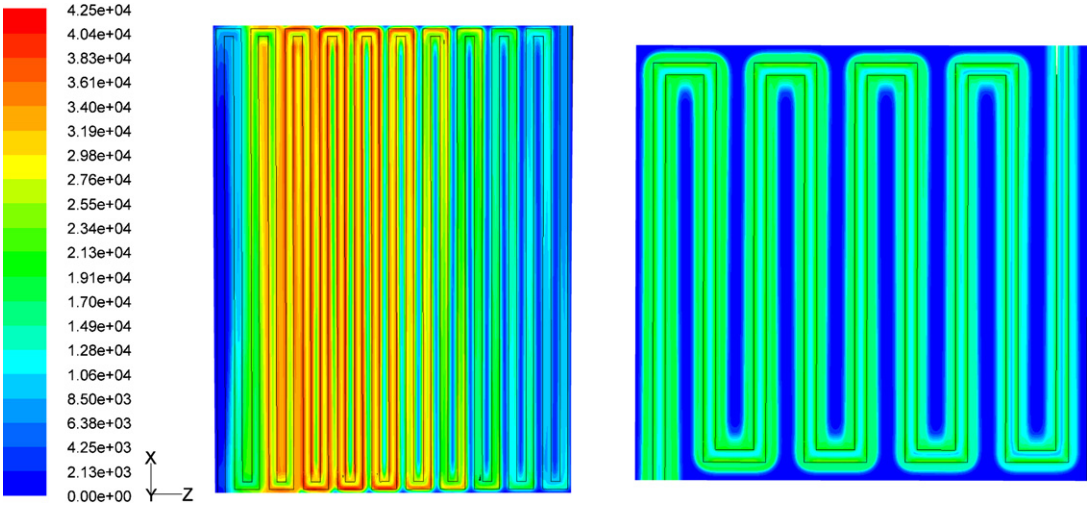

Fig. 7. Contour plots of current density (A m^{-2}) at the cathode GDL/CL interface for the best (left) and worst (right) individuals.

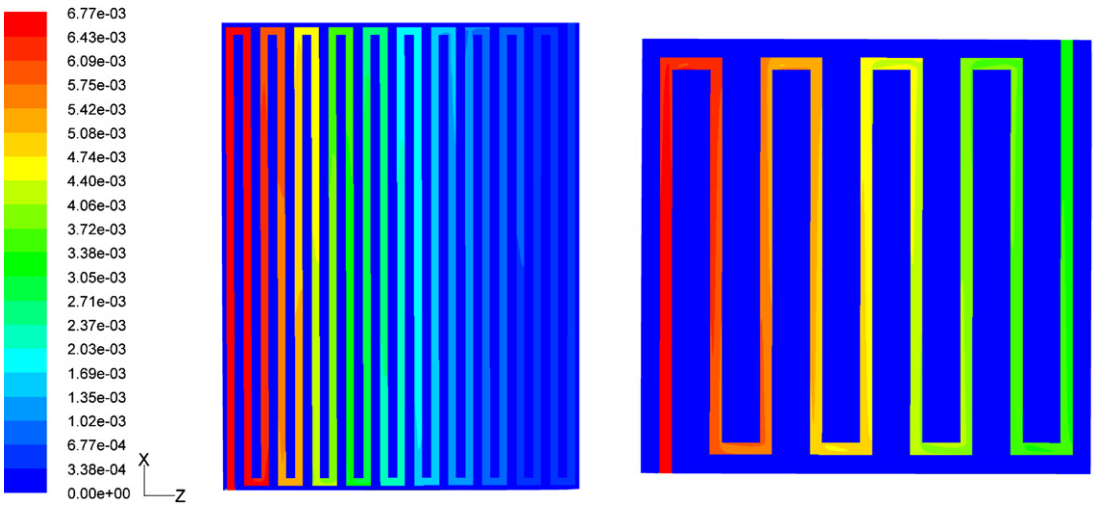

Fig. 8. Contour plots of oxygen concentration (kmol m^{-3}) along the cathode channel for the best (left) and worst (right) individuals.

the lands. According to Darcy's Law, convective bypass through the GDL is inversely proportional to the width of the land region. Hence, a large land width can severely inhibit convective bypass even in the presence of a significant pressure differential. The large land width of 3.5 mm for the worst case individual is responsible for extended dead zones under the lands and poor overall performance.

In addition, the reaction can proceed only if there is an adequate proton flux through the membrane from the anode side to complete the reaction on the cathode side. If the hydrogen concentration is depleted such as near the hydrogen outlet, then not enough hydrogen is convectively forced into the GDL and the reaction rate and current production are weak. The occurrence of such dead zones should be minimized as much as possible. Fig. 9 shows that there is still a significant concentration of hydrogen at the outlet of the worst performer, while the hydrogen is almost completely depleted by the time the flow reaches the outlet of the best individual.

The contour plot of oxygen concentration in three layers (top, middle and bottom) of the cathode GDL in Fig. 10 shows that there is oxygen under both the channel and the land for the best performer. This figure also shows that oxygen is driven towards the catalyst layer by the concentration gradient of oxygen in the *y*-direction. Oxygen diffuses through the thickness of the GDL parallel to the *y*-axis and is consumed directly below the channels. In addition, oxygen is also being delivered to the catalyst under the land areas.

The velocity vectors in Fig. 11 provide evidence that air is driven by convection under the ribs of adjacent passes for the best performer. Therefore, oxygen is delivered effectively to the catalyst layer even below the land areas. This is a desirable result because all of the catalyst area is able to participate in the reaction. In contrast, the velocities under the cathode lands in the case of the worst individual are not very high, implying that diffusion is the dominant transport mechanism for oxygen. Diffusion is not as effective in transporting reactant gas under the lands, and therefore, although the oxygen concentration is high under the channels for the worst individual, it experiences low oxygen concentration under the lands. Contrary to this result, the best performer shows evidence of both diffusive and convective transport.

The absolute pressure distribution within the channels and the GDL provides insight into the velocity distributions found in the GDL. Fig. 12 presents the pressure distribution along the midplane of the cathode GDL for the best and worst performers. As expected, the pressure gradients are highest in the vicinity of the channel roots at each pass. In the best individual, the pressure gradient is very effective at driving convective bypass under the land areas of the cell. The worst individual suffers because the pressure gradient

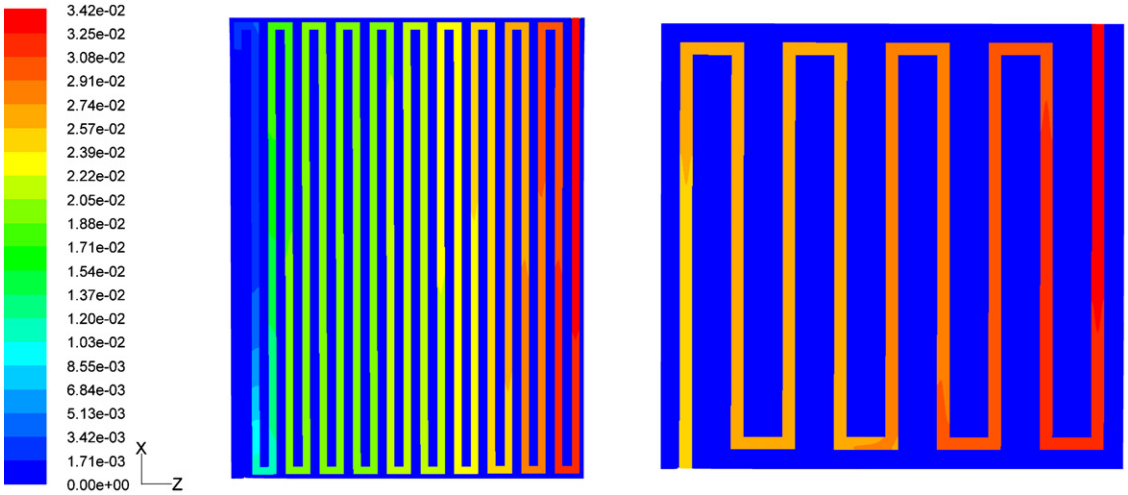

Fig. 9. Contour plots of hydrogen concentration (kmol m^{-3}) along the anode channel for the best (left) and worst (right) individuals.

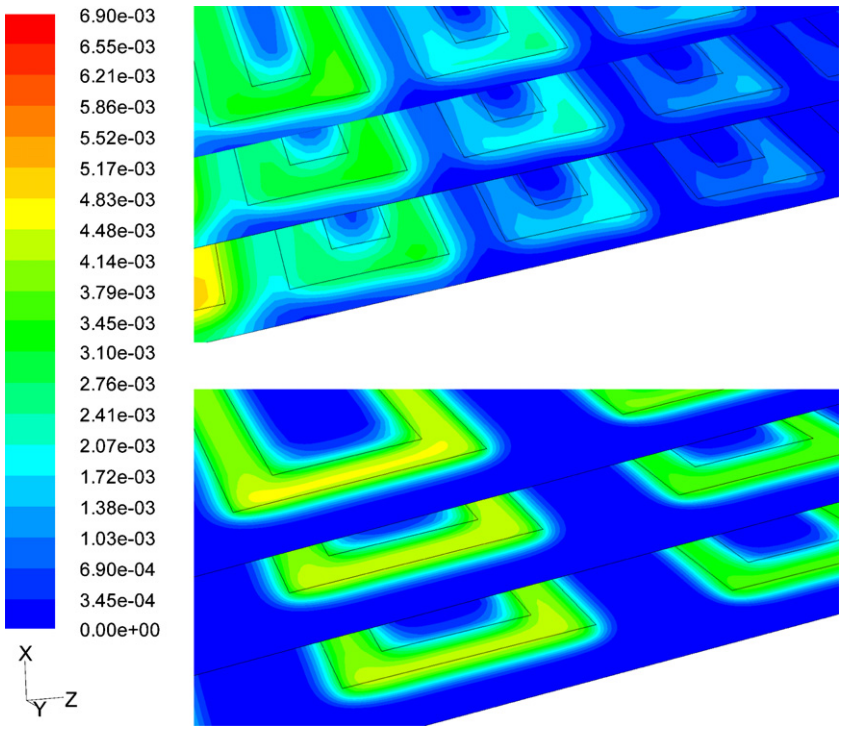

Fig. 10. Oxygen concentration (kmol m^{-3}) at the top, middle, and bottom of the cathode GDL for the best (top) and worst (bottom) performers. The bottom of the GDL is in contact with the catalyst layer.

is insufficient to drive convective bypass across the wide lands. The overall pressure difference across the worst case cell is small owing to the small number of passes, and hence the small total channel length. The pressure distribution is an important indicator of the cell's performance. The pressure distribution is mainly determined by the configuration of the gas flow channels. This result further validates the usefulness of this study to determine the optimal channel configurations for a specified cell area.

5.2. Comparison to neighbors

The data presented thus far have shown that, of a given set of individuals, there is clearly one that performs the best. The preceding discussion has also helped to explain the mechanisms that contribute to its good performance. Keeping in mind that the set of individuals that was actually evaluated by the GA is just a small subset of all the possible individuals the search space encompasses,

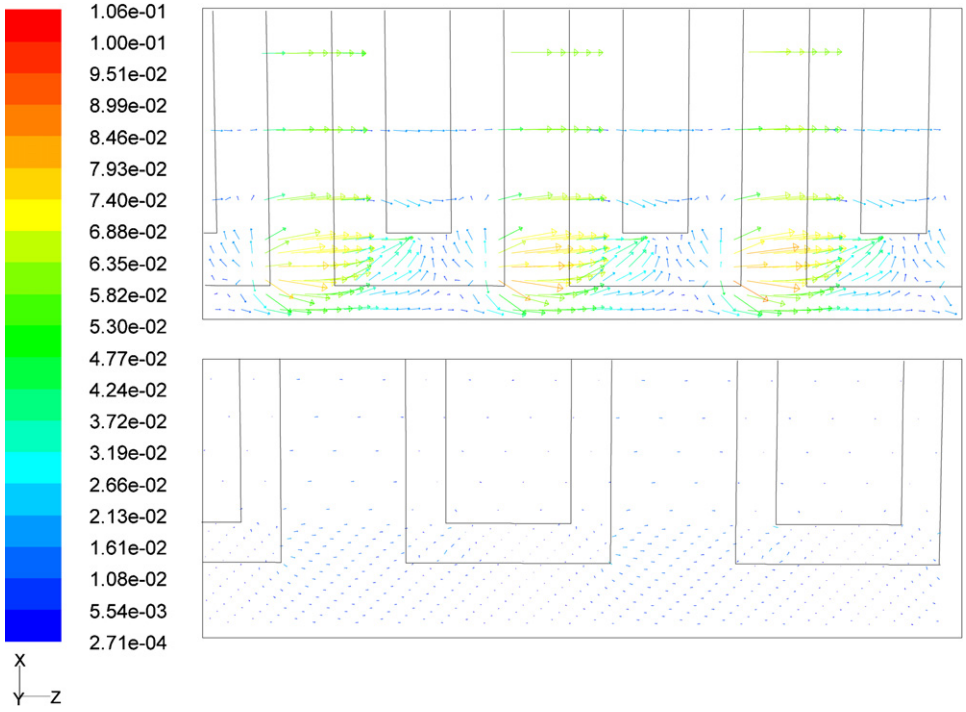

Fig. 11. Velocity vectors (m s^{-1}) along the midplane of the cathode GDL for the best (top) and worst (bottom) individuals.

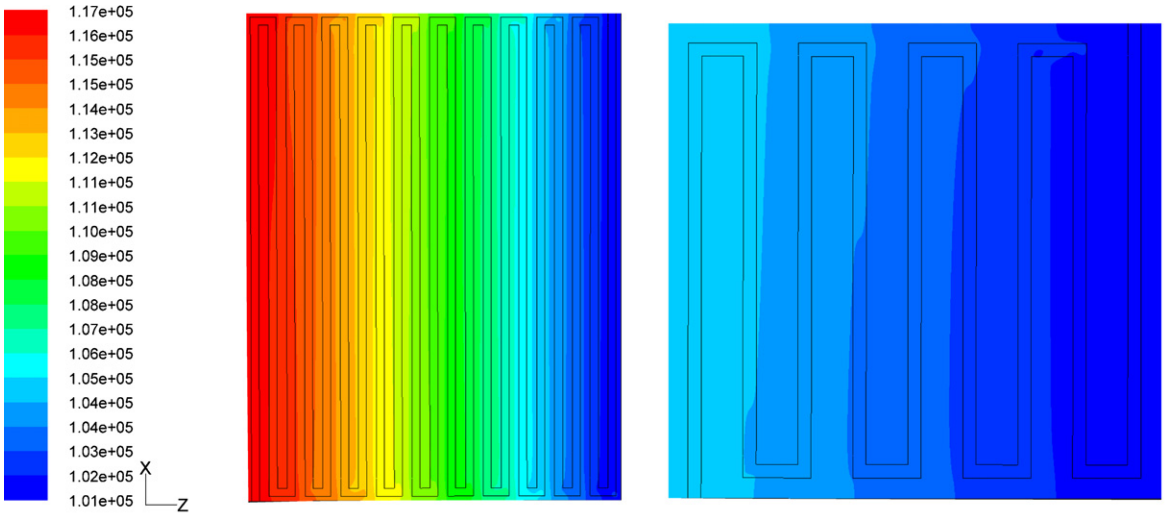

Fig. 12. Absolute pressure (Pa) along the midplane of the cathode GDL for the best (left) and worst (right) performers.

it is necessary to provide more evidence that the "best" individual is indeed the best of all possible individuals. The only way to prove this conclusively is to perform an exhaustive study of all of the combinations of the parameter values. This type of brute-force study is prohibitively expensive, and the GA technique was chosen in the first place to precisely avoid such an exercise. A simpler approach is to examine neighboring individuals with parameter values adjacent to those of the best individual and thereby confirm that the best individual is superior to its neighbors. Ideally, the GA should have ignored such inferior individuals and converged to the best individual. Accordingly, a "bracketing" study was performed in which each parameter value was varied from the optimum value by ±5% and ±10% while keeping the other parameter values fixed. The bracketing study resulted in 12 new individuals for whom the corresponding fitness values were evaluated. The performance of the new individuals is compared with the best performer in Fig. 13.

Fig. 13 shows that while all of the new individuals performed well, none was able to out-perform the best individual. This plot has two interesting characteristics. First, the GA did indeed correctly identify the best individual within this parametric "bracketing" study. Second, the best performer occupies the peak of a relatively flat performance region. The neighbors surrounding the best individual show a performance drop of no more than 2% of the optimal configuration. This observation suggests that while performing the study on this size of a PEMFC, it is important to isolate channel parameters that are near the optimum value, and that being close to the best performer is also a very good result.

5.3. Parasitic pumping losses

Upon inspecting Fig. 14, it becomes obvious why the fitness function was chosen to include the parasitic power losses associated with driving air through the cell. The parasitic power loss does not vary monotonically with the gross power output of the cell; i.e., a ranked order of best performers by net power would not be identical to a similar list ranked by gross power. This is because for a given cell area, the channel configuration can take on various channel geometries. The narrower the channel cross-sectional area

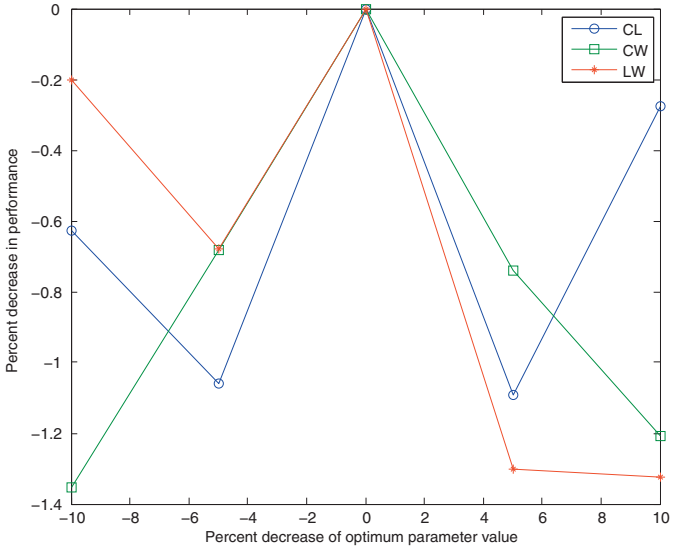

Fig. 13. Result of a bracketing study that compares the performance of neighbors with that of the best individual.

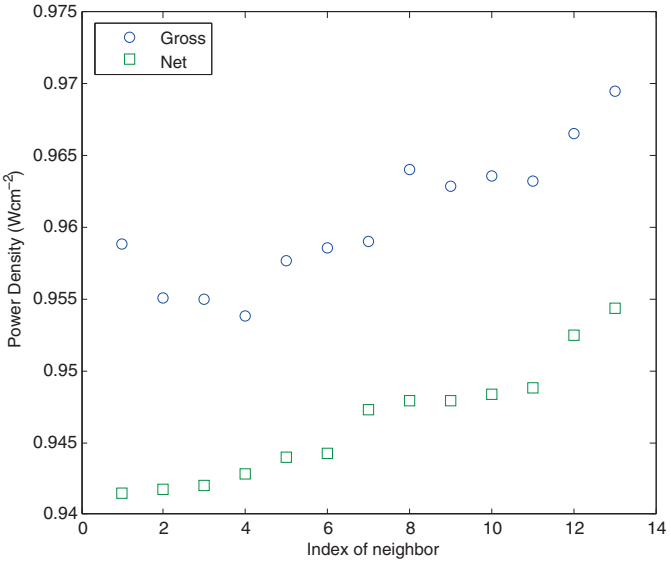

Fig. 14. Comparison of gross and net power density between the best individual and its neighbors.

and the longer the overall channel length, the higher the pumping requirements of the cell. Therefore, it is necessary to account for the parasitic power losses to accurately gauge PEMFC performance.

6. Conclusions

This research has focused on the optimization of a three-parameter single-serpentine channel configuration using the genetic algorithm method. The best possible individual, identified as the candidate with the highest net power density, was automatically determined by the GA and reasons for its superior performance were discussed. The GA was proven to effectively search a space for the best individual by means of a bracketing study which demonstrated that the best performer is indeed superior to all its immediate neighbors in parameter space.

Through this research, a powerful method of incorporating the strengths of several commercially available software packages has been developed. The unique contribution of this work is the method to efficiently automate the optimization of a PEMFC for a specified application. This method has developed an interface to automate communication of inputs and outputs between GAMBIT, FLUENT, and the MatLab GA Toolbox. Each software package has a unique scripting language capable of producing the data flow required by the optimization process. The communication is accomplished through the combination of several scripts, written in-house, that utilize these coding languages as well as the command line.

GA optimization has proven to be an efficient tool for searching a relatively large search space for an optimal value. The algorithm was successful in correctly identifying the best individual even though the search space associated with this work yielded a relatively flat region for the value of the fitness function in its immediate neighborhood. Therefore, the optimization can be trusted to find an optimum relatively close to the global search space optimal value.

Some limitations of this project include the following important considerations. First, the PEMFC model employed here assumed single-phase flow. Multiphase flow was not considered in this PEMFC model in order to reduce model complexity and computational time. Second, the best individuals tended to consume all of the available reactants implying some degree of reactant starvation near the outlets. These cells could have benefited from a higher inlet mass flow rate such that the reactant utilization was not quite so high, as long as the increased pumping power did not cause the net power density of the cell to drop.

While the search space explored by this algorithm thus far is useful for lab-scale fuel cell evaluation and comparison, the real value is in its ability to find an optimal PEMFC design configuration of any size. By successfully demonstrating the optimization of laboratory-scale PEMFCs, the method can confidently be applied to fuel cells of a larger target area. It is expected that in larger cells, the physical mechanisms that govern PEMFC performance would yield different optimal parameter values. The method developed here is capable of including as many parameters as the user desires, including material properties. Such additional parameters may include, but are not limited to: channel height, GDL thickness, GDL porosity, GDL permeability, and channel taper.

A significant feature of the method developed here is that other types of flow fields can also be evaluated. Configurations such as parallel, interdigitated, and multiple serpentine channels can be incorporated using the Gmesh script developed for this study. As long as the same zones and boundary condition types are prescribed by the Gmesh script, the Fjou script is capable of evaluating the fitness of any PEMFC and its desired channel configuration. However, it is recommended that mesh refinement studies are conducted on new channel configurations to ensure proper convergence and solution accuracy.

Acknowledgements

This work was funded by a grant from the Federal Transit Administration. GC was also partially supported by the NSF IGERT Program.

References

[1] J.P. Feser, A.K. Prasad, S.G. Advani, Journal of Power Sources 162 (2) (2006) 1226–1231.
[2] D.H. Jeon, S. Greenway, S. Shimpalee, J.W. Van Zee, International Journal of Hydrogen Energy 33 (3) (2008) 1052–1066.
[3] J.P. Feser, A.K. Prasad, S.G. Advani, Journal of Power Sources 161 (1) (2006) 404–412.
[4] X.D. Wang, Y.Y. Duan, W.M. Yan, Journal of Power Sources 172 (1) (2007) 265–277.
[5] H.C. Liu, W.M. Yan, C.Y. Soong, F. Chen, H.S. Chu, Journal of Power Sources 158 (1) (2006) 78–87.
[6] C. Xu, T.S. Zhao, Electrochemistry Communications 9 (3) (2007) 497–503.
[7] F. Chen, Y.Z. Wen, H.S. Chu, W. Ml Yan, C.Y. Soong, Journal of Power Sources 128 (2) (2004) 125–134.
[8] A.D. Le, B. Zhou, Journal of Power Sources 182 (1) (2008) 197–222.
[9] G. Hu, J. Fan, S. Chen, Y. Liu, K. Cen, Journal of Power Sources 136 (1) (2004) 1–9.
[10] D. Spernjak, A.K. Prasad, S.G. Advani, Journal of Power Sources 170 (2) (2007) 334–344.
[11] C.Y. Wang, S. Um, K.S. Chen, Journal of Electrochemical Society 147 (12) (2000) 4485–4493.
[12] S. Gottesfeld, T.E. Springer, T.A. Zawodzinski, Journal of Electrochemical Society 138 (8) (1991) 2334–2342.
[13] Fluent Inc. User's guide for GAMBIT Version 2.4.6. Fluent Inc., 2000.
[14] Fluent Inc. User's guide for FLUENT Version 6.3.26. Fluent Inc., 2006.
[15] S.N. Sivanandam, S.N. Deepa, Introduction to Genetic Algorithms, Springer, 2007.
[16] J. Larminie, A. Dicks, Fuel Cell Systems Explained, Wiley, 2003.